Available online at www.sciencedirect.com
ScienceDirect
International Journal of Refrigeration 30 (2007) 230–244
REVUE INTERNATIONALE DU FROID
INTERNATIONAL JOURNAL OF
refrigeration
www.elsevier.com/locate/ijrefrig

Air-side performance of a wavy-finned-tube direct expansion cooling and dehumidifying air coil

A.S. Huzayyin, S.A. Nada*, H.F. Elattar

Mechanical Engineering Department, Benha High Institute of Technology, Benha 13512, Egypt

Received 26 February 2006; received in revised form 16 July 2006; accepted 30 July 2006
Available online 27 October 2006

Abstract

Airside heat and mass transfer and fluid flow characteristics of a wavy-finned-tube direct expansion air coil under cooling and dehumidifying condition have been experimentally investigated. Experiments were carried out to study the effects of operating conditions such as: air temperature, air relative humidity, air face velocity, and evaporator pressure on the airside performance (cooling capacity, dehumidification capacity, pressure drop, and heat transfer coefficient) of the coil. Charts for coil wet conditions, partially wet or totally wet, were conducted to identify the coil wet conditions in terms of the operating conditions. Two techniques, enthalpy potential method and equivalent dry-bulb temperature method, were used to analyze the data and to deduce correlations for Colburn factors for the different coil wet conditions. Comparison between the correlations predictions of the two techniques was presented.

Keywords: Air conditioning; Evaporator; Finned tube; Experiment; Heat transfer; Mass transfer; Humid air; Pressure drop

Performance côté air d'un tube ondulé à ailettes dans le serpentin d'un système à détente directe en application refroidissement

Mots clés : Conditionnement d'air ; Évaporateur ; Tube aileté ; Expérimentation ; Transfert de chaleur ; Transfert de masse ; Air humide ; Chute de pression

1. Introduction

Finned tube heat exchangers are widely used in a variety of applications of air-conditioning, refrigeration and process industry. Air coil is an example of finned tube heat exchangers. Generally, air coils consist of tubes through which water, oils, or refrigerants are forced to flow inside the tubes while air is directed across the tubes. Since the dominate heat transfer resistance is usually on the air-side, using enhanced finned surface on this side is very common to effectively improve overall heat transfer performance. Air coils, heating or cooling, are usually employing different finned-tube configurations. Extensive investigations have been performed for wavy-finned-tube air coils under air-side dry condition to study the effects of the fins geometrical parameters

* Corresponding author. Tel.: +2012 1723182; fax: +2013 3230297.
E-mail address: samehnadar@yahoo.com (S.A. Nada).

0140-7007/$35.00 © 2006 Elsevier Ltd and IIR. All rights reserved.
doi:10.1016/j.ijrefrig.2006.07.023

Nomenclature

A	Area (m^2)
A_f	fins heat transfer surface area (m^2)
A_{fr}	coil air frontal flow area (m^2)
A_{min}	minimum air flow area (m^2)
A_o	total coil surface area (m^2)
A_t	tubes heat transfer outer surface area (m^2)
Cp_a	specific heat of moist air ($Cp_a = Cp_{da} + \omega\ Cp_v$) ($J\,kg^{-1}\,K^{-1}$)
$Cp_{a,i}$	specific heat of moist air at coil inlet ($J\,kg^{-1}\,K^{-1}$)
$Cp_{a,o}$	specific heat of moist air at coil outlet ($J\,kg^{-1}\,K^{-1}$)
Cp_{da}	specific heat of dry air ($J\,kg^{-1}\,K^{-1}$)
Cp_v	specific heat of water vapour ($J\,kg^{-1}\,K^{-1}$)
C_{PW}	parameter defined for partially wet condition by Eq. (11) (dimensionless)
C_W	parameter defined for totally wet condition by Eq. (5) (dimensionless)
D_h	coil hydraulic diameter ($D_h = 4L_d\,A_{min}/A_o$) (m)
G_{min}	maximum air mass velocity based on minimum flow area ($kg\,m^{-2}\,s^{-1}$)
h	heat transfer coefficient ($W\,m^{-2}\,K^{-1}$)
h_{ow}	total heat transfer coefficient (air–water film heat transfer), calculated based on enthalpy potential difference method ($W\,m^{-2}\,K^{-1}$)
h_{pw}	heat transfer coefficient under partially wet condition (calculated based on EDT method) ($W\,m^{-2}\,K^{-1}$)
h_{tw}	heat transfer coefficient under totally wet condition (calculated based on EDT method) ($W\,m^{-2}\,K^{-1}$)
h_w	heat transfer coefficient under wet condition (calculated based on enthalpy potential method) ($W\,m^{-2}\,K^{-1}$)
i	enthalpy ($J\,kg^{-1}$)
$i_{a,i}$	enthalpy of moist air at coil inlet ($J\,kg^{-1}$)
$i_{a,o}$	enthalpy of moist air at coil outlet ($J\,kg^{-1}$)
i_s	enthalpy of saturated air at tube surface temperature ($J\,kg^{-1}$)
J	Colburn factor (dimensionless)
J_{pw}	Colburn factor under partially wet conditions (calculated based on EDT method) (dimensionless)
J_{tw}	Colburn factor under totally wet condition (calculated based on EDT method) (dimensionless)
J_w	Colburn factor under wet conditions (calculated based on enthalpy potential method) (dimensionless)
k_f	thermal conductivity of fin material ($W\,m^{-1}\,K^{-1}$)
k_w	thermal conductivity of condensate water film ($W\,m^{-1}\,K^{-1}$)
L_d	coil depth (m)
M	parameter defined by Eq. (7) (m^{-1})
$\dot{m}_a$	air mass flow rate (dry air) ($kg\,s^{-1}$)
$\dot{m}_{cond}$	rate of water condensate ($kg\,s^{-1}$)
P_{evap}	evaporator gauge pressure (Pa)
Pr	Prandtl number (dimensionless)
ΔP_{coil}	air pressure drop across the coil (Pa)
$\dot{Q}$	rate of heat transfer (W)
$RH_{a,i}$	air relative humidity at coil inlet (dimensionless)
Re	Reynolds number based on hydraulic diameter ($Re = G_{max}D_h/\mu$) (dimensionless)
r_i	radius from tube center to fin base (m)
r_o	radius from tube center to fin tip (m)
St	stanton number ($St = h/(G_{max}C_{p_a})$) (dimensionless)
$T_{a,dew}$	air dew point temperature (°C)
$T_{a,i}$	air dry-bulb temperature at coil inlet (°C)
$T_{a,o}$	air dry-bulb temperature at coil outlet (°C)
$T_{a,ie}$	equivalent air inlet dry-bulb temperature (°C)
T_{avf}	average fin temperature (°C)
T_{ftip}	fin tip temperature (°C)
T_{ftipc}	critical temperature to differentiate partially wet and totally wet modes (°C)
T_s	tube surface temperature (°C)
ΔT	air temperature drop across coil ($\Delta T = T_{a,o} - T_{a,i}$) (°C)
$V_{a,i}$	air coil face velocity ($m\,s^{-1}$)
$w_{a,i}$	humidity ratio of moist air at coil inlet ($kg_v\,kg_a^{-1}$)
$w_{a,i}$	humidity ratio of moist air at coil outlet ($kg_v\,kg_a^{-1}$)

Greek symbols

$\eta_{f,pw}$	partly wet fin efficiency (dimensionless)
$\eta_{f,tw}$	totally wet fin efficiency (dimensionless)
η_{fw}	wet fin efficiency (dimensionless)
δ	fin thickness (m)
ϕ	parameter defined by Eq. (8) (dimensionless)
μ	dynamic viscosity ($N\,s\,m^{-2}$)

and number of tubes rows on the coil performance [1–8]. Relatively, researches on cooling and dehumidifying air coils are quite limited due to the complication of simultaneous heat and mass transport of the moist air over the coil surface. Most of these studies [9–16] have been conducted on plate-finned tube chilled water coils. Similar study has been carried out by Theerakulpisut and Priperm [17] for plate-finned tube direct expansion air coil. Effects of fins

geometrical parameters and number of tube rows on fluid flow and heat transfer characteristics were the aim of these studies. Very limited researches on the performance of wavy-finned-tube cooling and dehumidifying chilled water air coils are available. Mirth and Ramadhyani [18,19] have carried out experimental and numerical works, respectively, to predict the performance of five samples of wavy-finned-tube chilled water cooling coils under dry and wet conditions. Later Lin et al. [20] carried out an experimental study on the airside performance of herringbone wavy-finned-tube air coils in wet conditions. Correlations of Nusselt number were developed.

Traditionally, air coils under dehumidification condition are analyzed by the enthalpy potential difference approach assuming that the entire coil surface is covered by a vapour condensate layer of uniform thickness [21]. However, under different operating conditions, the coil surface may have three different modes of wet conditions. These modes are totally wet, partially wet and totally dry coil surface conditions. When the air dew point temperature is equal to or greater than the fins tip temperature, all fins and tube surfaces are wetted and the coil becomes under a totally wet condition. When the air dew point temperature lies between the fins tip temperature and the tube surface temperature (fins base temperature), only part of fins surfaces are wetted and the coil becomes under a partially wet condition. When the air dew point temperature is smaller than the tube surface temperature (fins base temperature) no condensation occurs and the coil is under a totally dry condition. Fig. 1 shows these different modes on the Psychrometric chart. Basically, fins performance depend on the fin wet conditions; dry, totally wet or partially wet fins [22–25]. Thus a large error is expected if the coil is analyzed by the enthalpy potential difference approach without distinguish between the different coil wet conditions modes. More recently, Wang and Hihara [26] have described a new method, equivalent dry-bulb temperature (EDT) method, to predict the airside coil performance under dry, partially wet and totally wet cooling conditions. In this method, an equivalent dry process, process 1_e–2_e–3 (for the partially wet condition as an example) with identical cooling capacity of the actual process, process 1–2–3, is assumed (see Fig. 1). Doing this, the heat transfer characteristics of the coil were analyzed based on the temperature difference ($T_{1e} - T_s$). Different equations for predicting fin surface efficiency were used in the analysis of the different coil wet conditions. Wang and Hihara [26] have used this method (EDT) to predict the heat and mass transfer rates and the coil wet conditions of previous experimental data of plain-finned tube coils which have been analyzed by the enthalpy potential method.

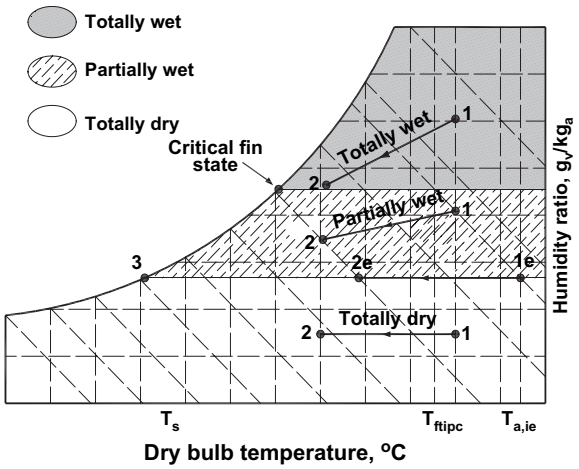

Fig. 1. Different cooling modes.

The present literature review reveals that most of the previous investigations have not studied the effects of the operating conditions (air temperature, air relative humidity, and evaporator pressures) on the airside performance of the cooling and dehumidifying coils. Moreover, most of the previous investigations analyzed the heat transfer characteristics of the cooling and dehumidifying coils using the enthalpy potential method without distinguish between the different coil wet conditions. In addition to that, most of these studies were carried out on plain-finned-tubes chilled water coils. Investigations on direct expansion wavy-finned tube air coils are very limited. Therefore, the present study aims to study the effects of the operating conditions (air temperature, air relative humidity, air velocity, and evaporator pressure) on the airside performance of a direct expansion wavy-finned tube air cooling and dehumidifying coil using R134a as a refrigerant. The operating conditions were chosen to obtain different coil wet conditions (partially wet or totally wet). The equivalent dry-bulb temperature method was used to characterize the heat transfer for each coil wet condition. Moreover, the traditional enthalpy potential difference method was used to characterize heat transfer for all data as an aim to evaluate and compare the two methods.

2. Experimental setup and procedure

2.1. Experimental setup

The experimental setup is shown schematically in Fig. 2a. It consisted of three sections: wind tunnel, refrigeration circuit, and tested air coil. The tunnel was an open circuit, delivery type rectangular duct of 390 mm (width) × 335 mm (height) and had an overall length of 5130 mm. Air was forced through the tunnel using upstream variable speed centrifugal fan. The fan was connected to the diverging section of the tunnel through a flexible section to avoid noise and vibration of wind tunnel. The tunnel walls were thermally insulated by 1-inch thick glass wool insulation. The air, delivered from the fan, flow through the following tunnel sections: heating section, humidification section, mixing and turbulence eliminating sections and test coil section. The heating and humidification sections were used to adjust the air temperature and humidity at the coil entrance

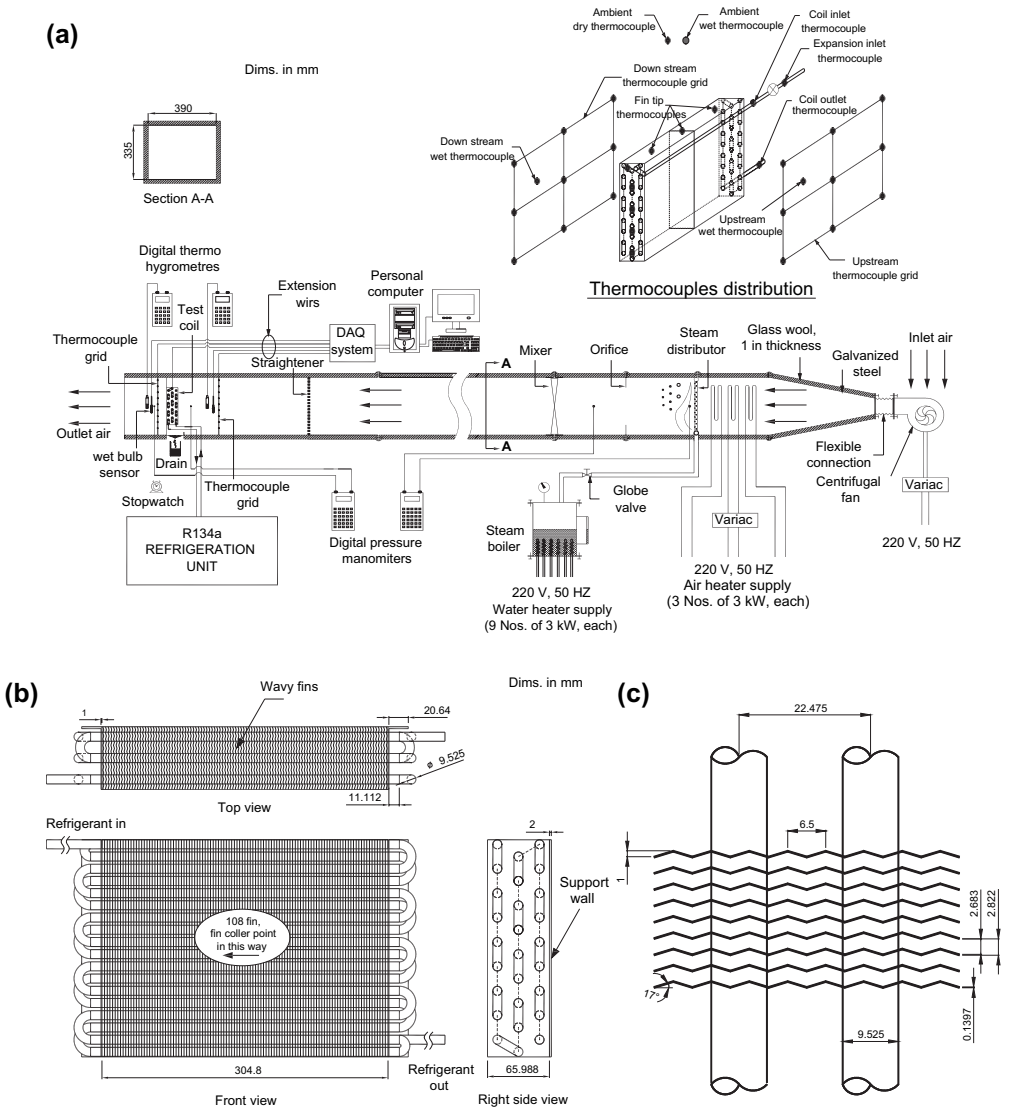

Fig. 2. (a) Schematic diagram of experimental setup and thermocouples distribution, (b) test coil views, and (c) geometry of wavy fins.

to the required value. The heating section consisted of three electric heaters; each had a power of 3 kW. Each heater was made from 3 m steel bare of 8.5 mm diameter and formed in serpentine shape. The heaters were in staggered arrangement to cover the entire duct cross section area. The intermediate heater was connected to a variac to smoothly control the air temperature. The humidification section consisted of five parallel vertical aluminum tubes (diameter = 16 mm), each tube had 38 holes of 2 mm diameter uniformly distributed along and around the axis and circumference of the tube. The tubes were connected to an aluminum header (diameter = 25 mm) from each side. Humidifier dimensions were chosen to cover the entire cross section of the tunnel to obtain uniform humidity distribution. Steam was supplied to the humidifier from an electrical boiler that had nine electrical heaters, 3 kW each. The rate of steam flowing through the humidifier was controlled by mean of a globe valve and also by controlling the power input to the electric boiler. The mixing and turbulence eliminating section was used to assure uniform air velocity and properties through the wind tunnel cross section at coil entrance. A flow straightener consisting of three layers of mesh screen was placed down stream the mixing section to eliminate the flow turbulences.

The test coil was a wavy-finned tube air coil of 304.8 mm × 228.6 mm face area and had three tubes rows in staggered arrangement (see Fig. 2b). The geometry and configurations of the wavy fins with respect to the

coil tubes are shown in Fig. 2c. The physical data of the test coil are given in Table 1. Refrigerant 134a, originally coming from the refrigeration circuit, passes inside the tubes of the coil, while air coming from the tunnel passes through the fins of the air coil in cross flow arrangement with the coil tubes. A basin with a collecting and measuring tank was placed under the air coil to collect and measure the condensate drain.

A refrigeration circuit was used to supply refrigerant R134a to the air coil. The main components of the refrigeration circuit were reciprocating compressor, oil separator, air cooled condenser, liquid receiver, filter and liquid indicators, heat exchanger, automatic expansion valve, back pressure regulator, suction line accumulator and evaporator (tested air coil). Further details of the experimental set up are given in Elattar [27].

2.2. Measuring instruments and calibration method

Measuring instruments were used to measure the physical quantities which are necessary to study the coil performance. As shown in Fig. 2a, two groups of thermocouples, each contains nine thermocouples, were used to measure the air temperatures (dry-bulb) distributions through the wind tunnel cross sections just upstream and downstream the coil. Two other thermocouples (placed in continuously wetted cotton bulb) were used to measure the air wet bulb temperatures just upstream and downstream the coil. Another eleven thermocouples were used to measure the coil surface temperatures at different locations: the refrigerant inlet and exit pipes of the coil, fins tips, the refrigerant pipe surface at the entrance of the expansion device and the surface of the coil tube (five thermocouples were attached on coil tubes surfaces). Two other thermocouples were used to measure the ambient dry and wet bulb temperatures. All thermocouples were 0.5 mm K-type (Chromel–Alumel). All thermocouples were connected to a data acquisition system and a PC through extension wire to record thermocouples readings. The thermocouples were calibrated using standard thermometer of accuracy ±0.2 °C. An orifice meter with a digital differential pressure manometer with accuracy ±0.1 Pa was used to measure the air flow rate by measuring the pressure drop across the orifice. The orifice meter was calibrated by measuring the air velocity distribution through the tunnel cross section using a hotwire anemometer and at the same time recording the pressure drop across the orifice. Equal area traverses method was used to calculate the average air velocity over the duct cross section area and consequently the air flow rate. The air pressure drop across the coil was measured by another digital differential pressure manometer with accuracy ±0.1 Pa. Two digital Thermo Hygrometers of measuring ranges (5–98% RH) with resolution (±0.1% RH) were used to measure the air relative humidity just upstream and downstream the coil. Six pressure gauges of different ranges were used to indicate the refrigerant pressure at inlets and outlets of the compressor, the condenser, and the evaporator. Another pressure gauge was used to indicate the boiler pressure.

Table 1
Coil geometric parameters

Coil dimensions	
Coil face width	304.8 mm
Coil face height	228.6 mm
Coil deep	65.989 mm
Coil face area	0.06968 m^2
Coil actual flow area	0.041395 m^2
Coil total external surface area	3.2621 m^2
Tubes specifications	
Number of tube rows	3
Number of tubes in each row	9
Tube material	Copper
Tube arrangement	Staggered
Length of straight tube	304.8 mm
Transverse tube spacing	22.475 mm
Longitudinal tube spacing	25.715 mm
Outside tube diameter	9.525 mm
Inside tube diameter	8.712 mm
Fins specifications	
Type	Wavy
Material	Aluminum
Thickness	0.1397 mm
Collar diameter	9.8044 mm
Number	108
Pitch	9 fins/inch
Wavelength	6.5 mm
Wave height	1 mm
Corrugation angle	17°

2.3. Experimental conditions

The ranges of the test variables used in this study were:

Air inlet temperature	20–30 °C
Air inlet relative humidity	40–95%
Frontal air velocity	0.5–1.5 m s^{-1}
Evaporator gauge pressure	308–377 kPa.

3. Data reduction

The airside performance of the test coil was measured by the dimensionless Colburn factor (J) that characterizes the airside heat transfer coefficient. The heat transfer rate through the coil surface and the dehumidification capacity were calculated from the measurements of the air properties just upstream and downstream the coil as follows

$$\dot{Q} = \dot{m}_a(i_{a,i} - i_{a,o}) \quad (1)$$

$$\dot{m}_{cond} = \dot{m}_a(\omega_{a,i} - \omega_{a,o}) \quad (2)$$

In the analysis of the present data, two techniques were used to calculate the airside heat transfer coefficient. The first one is the conventional enthalpy potential method technique (Threlkeld [21]). The second technique, recently presented by Wang and Hihara [26], is the equivalent dry-bulb temperature technique (EDT).

3.1. Enthalpy potential method

In analyzing the data using the enthalpy potential method, the total heat transfer coefficient was calculated from Eqs. (3)–(5) [21]

$$\dot{Q} = \frac{h_{ow}}{C_w Cp_a}\left(A_s + \eta_{f,w} A_f\right)(i_{a,i} - i_s), \tag{3}$$

$$h_{ow} = \frac{1}{\left(\frac{1}{h_w C_w} + \frac{y_w}{k_w}\right)} \tag{4}$$

$$C_w = \frac{di/dT}{Cp_a} \quad \text{at } T = T_{avf} \tag{5}$$

In Eq. (4), the condensate film thickness, y_w, was assumed 0.127 mm as recommended by many previous investigators [12,21,23,26]. The wet fin efficiency was calculated by Eqs. (6)–(8) that recommended by many previous investigations (see Hong and Webb [23] and Wang and Hihara [26]).

$$\eta_{f,w} = \frac{\tanh(Mr_i\phi)\cos(0.1Mr_i\phi)}{Mr_i\phi} \tag{6}$$

$$M = \left(\frac{2h_w C_w}{k_f \delta}\right)^{0.5} \tag{7}$$

$$\phi = \left[\frac{r_o}{r_i} - 1\right]\left[1 + 0.35\ln\left(\frac{r_o}{r_i}\right)\right] \tag{8}$$

In Eq. (8), the fin area served by each tube was assumed to be equivalent in performance to a flat circular-plate fin of equal area [23].

3.2. Equivalent dry-bulb temperature (EDT) method

According to the air dew point temperature relative to the coil surface temperature distribution, two different coil wet conditions were obtained in the present experiments; namely totally wet and partially wet coil conditions. Totally wet occurred when the air dew point temperature was equal to or greater than the fins tip temperature, i.e. $T_{adew} \geq T_{ftip}$. Partially wet conditions occurred when the air dew point temperature lies between the fins tip temperature and the fins base temperature, i.e. $T_s < T_{adew} < T_{ftip}$. Since T_{adew}, T_s and T_{ftip} depend on the operating conditions (air temperature, air relative humidity, air Reynolds number and evaporator pressure), the existence of a partially wet or totally wet condition depends on these operating conditions. Therefore, measurements of T_{adew}, T_s and T_{ftip} in each experiment were used to determine if the operating conditions of this experiment give partially wet or totally wet condition. After the determination of the coil wet conditions to all experiments, cooling mode charts were conducted. Fig. 3 shows the cooling and dehumidification mode charts obtained from the present experimental data. As shown in Fig. 3, totally wet conditions probably occur at high relative humidity and air temperatures and low evaporator pressures and air velocities.

EDT method was proposed by Wang and Hihara [26] to calculate the heat transfer coefficients under totally wet and partially wet coil conditions. To simplify the analysis and deduce correlations which can be used directly to predict the coil performance of a direct expansion coils in terms of the evaporator pressure, the tube surface temperature was considered to be uniform and equal to the saturation temperature of the refrigerant. The heat transfer coefficients for totally wet and partially wet coil conditions were calculated from Eqs. (9) and (10), respectively [26].

$$\dot{Q} = h_{tw}\left(A_t + \eta_{f,tw}A_f\right)(T_{a,ie} - T_s) \tag{9}$$

$$\dot{Q} = h_{pw}\left(A_t + \eta_{f,pw}A_f\right)(T_{a,ie} - T_s) \tag{10}$$

where, $T_{a,ie}$ is the equivalent dry-bulb temperature of inlet state (see Fig. 1). The fin efficiency at totally wet condition is calculated from Eqs. (6)–(8) and h_w in Eq. (7) is replaced by h_{tw}. Also the fin efficiency under partially wet conditions is calculated from Eqs. (6)–(8) and h_w in Eq. (7) is replaced by h_{pw} and C_w in Eq. (7) is replaced by C_{pw} that defined as follow [26].

$$C_{pw} = 1.0 + \left[\frac{C_w - 1}{T_{a,ie} - T_{ftipc}}\right](T_{a,ie} - T_{a,i}) \tag{11}$$

where T_{ftipc} is the temperature of the projection of the critical fin state on the constant enthalpy line that pass by state 1 (see Fig. 1).

The Colburn factor (J) is the main parameter that characterizes the airside heat transfer coefficient in a dimensional form. It was calculated by Eqs. (12) and (13)

$$J = StPr^{2/3} \tag{12}$$

$$St = \frac{h}{G_{max} Cp_a} \tag{13}$$

where, (h and J) is (h_w and J_w) in the analysis of the enthalpy potential method and are (h_{tw} and J_{tw}) and (h_{pw} and J_{pw}) in the analysis of the EDT method for totally wet and partially wet conditions, respectively.

A computer program was developed to solve Eqs. (1)–(13) to find the J factor (using both of enthalpy potential method and EDT method). Eqs. (1)–(13) can be put on the form $J = f(x_1, x_2, x_3, \ldots, x_n)$ where (x_1, x_2, x_3,…,x_n) are the measured parameters. The errors in the measurements of these parameters were ±0.2 °C for any temperature measurements, ±0.1 Pa for pressure measurements, ±0.1% for

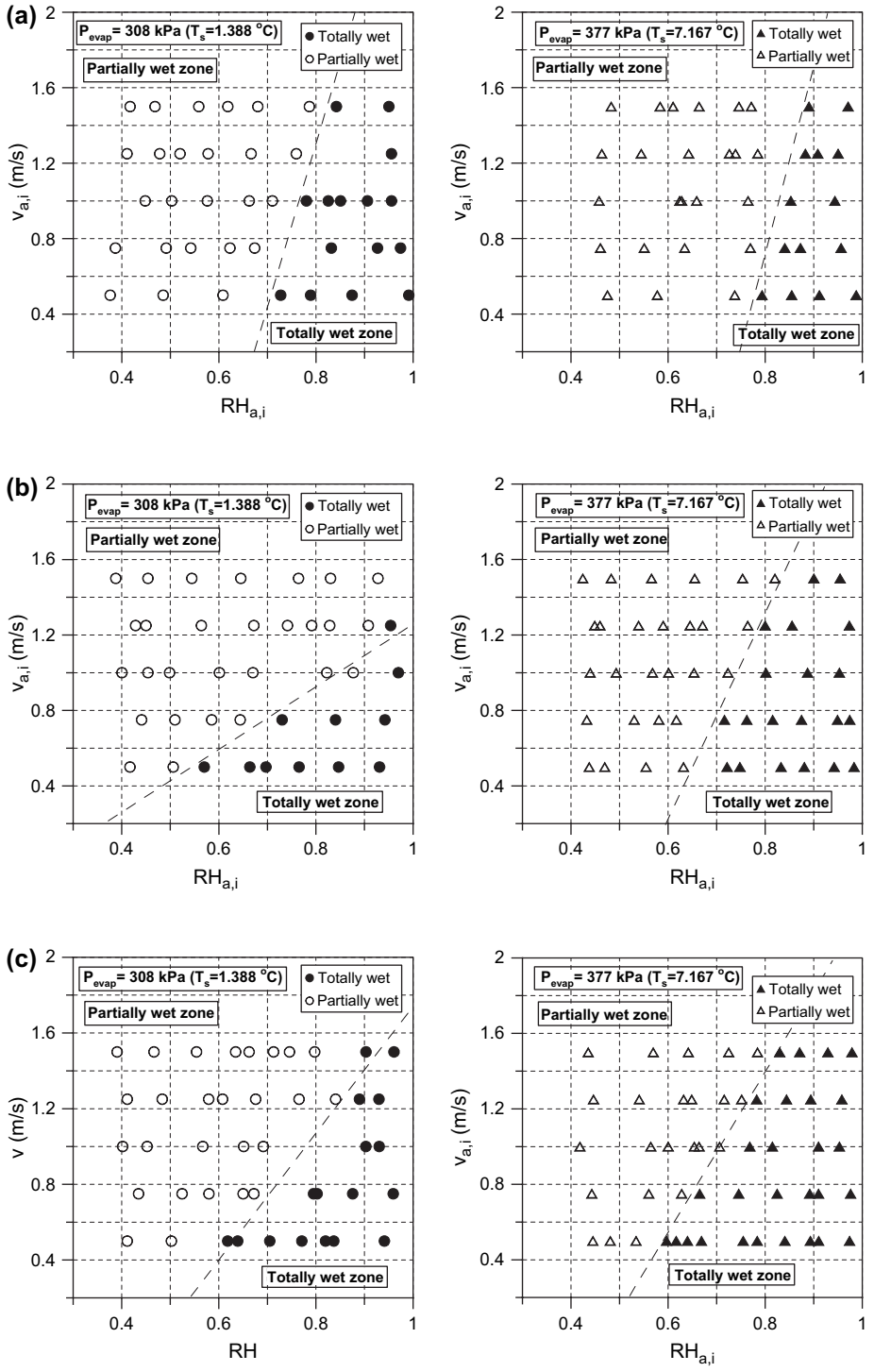

Fig. 3. Cooling modes charts. (a) $T_{a,i} = 20\ ^\circ C$, (b) $T_{a,i} = 25\ ^\circ C$, and (c) $T_{a,i} = 30\ ^\circ C$.

relative humidity measurements and $\pm 0.008\ \mathrm{m\,s^{-1}}$ for air velocity measurements. The uncertainty in J due to the uncertainties of these parameters can be calculated from Eq. (14) that was given by Holman and Gajda [28].

$$\frac{\Delta J}{J} = \left[\left(\frac{\partial J}{\partial x_1}\frac{\Delta x_1}{J}\right)^2 + \left(\frac{\partial J}{\partial x_2}\frac{\Delta x_2}{J}\right)^2 + \cdots + \left(\frac{\partial J}{\partial x_N}\frac{\Delta x_N}{J}\right)^2\right]^{1/2} \tag{14}$$

where $\partial J/\partial x_i$ was calculated by numerical differentiation using the developed computer program. The minimum and maximum uncertainty in J_w, J_{tw}, and J_{pw} for all the data were found to be (5.5 and 9.5%), (2 and 4%), and (2.5 and 9%), respectively.

4. Results and discussions

The results of the present work were presented to investigate the effects of the operating conditions: air coil face velocity, air relative humidity, air temperature and evaporator pressure on coil performance and characteristics. In the first part of this section, the effects of the operating conditions on the temperature drop across the coil, the coil dehumidification capacity and the pressure drop across the coil were presented and investigated. In the second part, the effects of the operating conditions on the heat and mass transfer characteristics were analyzed and discussed.

4.1. Effect of operating conditions on cooling and dehumidification capacities and pressure drop

4.1.1. Effects of air inlet relative humidity

Fig. 4a–c shows the variation of the cooling capacity (ΔT), dehumidification capacity ($\dot{m}_{cond}$) and the air pressure drop across the coil (ΔP_{coil}), respectively, against the air inlet relative humidity with the air coil face velocity as a parameter for $T_{a,i} = 20\ ^\circ\mathrm{C}$ and $P_{evap} = 308$ kPa (curves for other $T_{a,i}$ and P_{evap} are given in Elattar [27]). Fig. 4a shows that, for any air face velocity, ΔT significantly decreases with increasing the air inlet relative humidity. The trend is same for all evaporator pressures and air temperatures (see Elattar [27]). This trend can be attributed to the increase in the motive force of water vapour diffusion with the increase of the air relative humidity and this increases the number of water vapour molecules condensing on the tubes and fins surfaces. This increases the thermal resistance of the condensate layer. The increase of the thermal resistance of the condensate layer reduces the fins efficiency and this leads to a high fin and tube surface temperature and in consequently a high air exit temperature. This is supported by the results of Wang et al. [12] and Hong and Web [23] that showed the decrease of fin efficiency with increasing inlet air relative humidity.

Fig. 4b shows the increase of the dehumidification capacity ($\dot{m}_{cond}$) with increasing the air relative humidity for any air face velocity. This can be attributed to the increase of the vapour pressure of the air. Increasing the vapour pressure

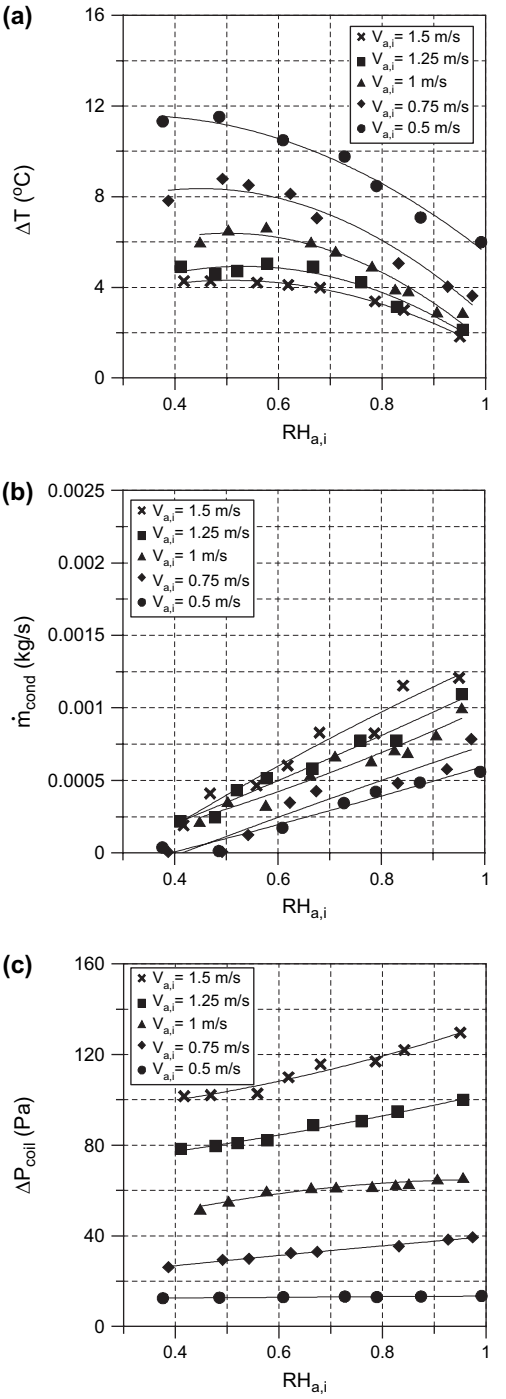

Fig. 4. Effect of $RH_{a,i}$ and $V_{a,i}$ on ΔT, $\dot{m}_{cond}$ and ΔP_{coil} ($T_{a,i} = 20\ ^\circ\mathrm{C}$ and $P_{evap} = 308$ kPa). (a) Effect on temperature drop across the coil, (b) effect on coil dehumidification capacity, and (c) effect on air pressure drop across the coil.

increases the potential of water vapour transfer to the cooling surface and this increases the dehumidifying capacity. The trend is the same for different evaporator pressures and air temperatures (see Elattar [27]).

Fig. 4c shows the increase of the air pressure drop across the coil with increasing the air relative humidity. The trend is the same for all air temperatures, air face velocities and evaporator pressures (see Elattar [27]). Increasing the air relative humidity increases the rate of water vapour condensation and this increases the area of the wet portions of coil surface and also increases the thickness of the condensate film formed on fins and tubes surfaces. These lead to higher surface roughness at the air coil interface and thinner free flow area of the air. Both cause the increase of the air pressure drop across the coil.

4.1.2. Effects of air coil face velocity

Fig. 4a–c shows also the effect of the air coil face velocity on the cooling capacity, dehumidification capacity and the pressure drop across the coil, respectively, for $T_{a,i} = 20\ ^\circ C$ and $P_{evap} = 308$ kPa (curves for other $T_{a,i}$ and P_{evap} are given in Elattar [27]). As shown in Fig. 4a, ΔT decreases with increasing the air face velocity. The trend is the same for all air temperatures and evaporator pressures. This trend can be attributed to the increase of air bypass across the coil surfaces with increasing air flow rate. Increasing the coil bypass factor increases the air outlet temperature. In contradictory, increasing the air face velocity increases the rate of heat transfer between the air contact to the coil and the coil surface. This leads to the decrease of the outlet air temperature but this reduction in the temperature cannot overcome on the increase of the air exit temperature due to the increase of the air bypass factor.

Fig. 4b shows the increase of the dehumidification capacity with increasing the coil face velocity. This can be attributed to the following: (1) increasing the air velocity increase the rate of mass transfer between the air and the coil surface and this increases the dehumidification capacity, and (2) increasing the air face velocity increases the process of renewing the air that in contact to the coil surface and this causes an increase in the dehumidification capacity. The trend is the same for all air temperatures and evaporator pressures (see Elattar [27]).

Fig. 4c shows the increase of the air pressure drop across the coil with increasing the air face velocity. This can be attributed to the following: (1) increasing the air face velocity increases the shear stress between the air and the coil surface and this significantly increases the pressure drop across the coil, and (2) as shown in Fig. 4b, increasing the air coil face velocity increases the dehumidification rate and this increases the pressure drop across the coil.

4.1.3. Effects of air inlet temperature

The effects of the air inlet temperature on the dehumidification capacity, cooling capacity, and the air pressure drop across the coil are shown in Fig. 5a–c, respectively, for air face velocity, and evaporator pressures of $1\ m\ s^{-1}$, and 308 kPa, respectively. As shown in Fig. 5a and b, the dehumidification capacity increases and the cooling capacity decreases as the air inlet temperature increases. This can be attributed to

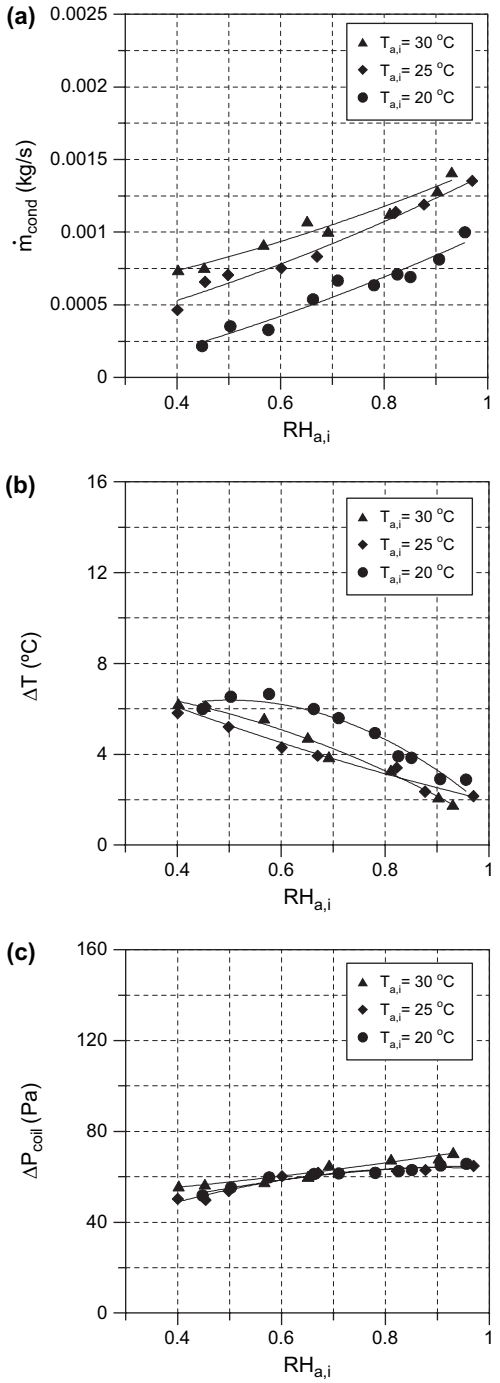

Fig. 5. Effect of air temperature on (a) dehumidification capacity, (b) temperature drop across the coil, and (c) air pressure drop across coil, at $V_{a,i} = 1\ m\ s^{-1}$ and $P_{evap} = 308$ kPa.

the increase of water vapour pressure with the increase of the air temperature for the same inlet relative humidity. Increasing the vapour pressure increases the potential difference that cause vapour transfer between air and coil surface and this increases the dehumidification capacity. Increasing the dehumidification capacity increases the latent heat transfer on the account of the sensible heat transfer and this causes a reduction in the air temperature drop across the coil. These results are consistent with the result of the theoretical analysis of Liang et al. [25] that showed the increase of the water condensation rate and the decrease of the air temperature drop across the coil with the increase of the air inlet temperature. Fig. 5c shows that the air temperature has approximately no effect on the air pressure drop across the coil.

4.1.4. Effects of evaporator pressure

Fig. 6a–c shows the effect of the evaporator pressure on the dehumidification capacity, cooling capacity and the air pressure drop across the coil for air velocity and air temperature of 1 m s^{-1} and 20 °C, respectively. As shown in Fig. 6a and b, the dehumidification and the cooling capacities increase as the evaporator pressure decreases. This can be attributed to the decrease of the coil apparatus dew point with the decrease of evaporator pressure. This is consistent with the results of the theoretical analysis of Liang et al. [25] that showed the increase of the coil air outlet temperature and the decrease of the water condensate rate with the increase of the coil saturation temperature. Fig. 6c shows that the evaporator pressure has approximately no effect on the air pressure drop across the coil.

4.2. Heat transfer characteristics

Fig. 7 shows the variations of h_w, J_w, J_{tw} and J_{pw} against *Re* with $RH_{a,i}$ as a parameter for $T_{a,i} = 20$ °C and $P_{evap} =$ 308 kPa (curves for other $T_{a,i}$ and P_{evap} are given in Elattar [27]). As shown in the figure, for the entire range of *Re*, h_w, J_w, J_{tw} and J_{pw} decrease with increasing the air relative humidity. The trend is the same for all evaporator pressures and air temperatures (see Elattar [27]). This trend can be attributed to the increase of the condensation rate with increasing the air relative humidity and this leads to higher fin and tube surface temperatures as a result of the increase of thermal resistance of the condensate layer and in consequently the decrease of the fins efficiency. Higher fin and tube surface temperatures lead to a lower heat transfer rate and in consequently a lower heat transfer coefficient and Colburn factor.

Fig. 7 also shows the increase of the heat transfer coefficient and the decrease of the Colburn factor with increasing *Re*. The trend is the same for all evaporator pressures, air temperatures and relative humidity. The increase of the heat transfer coefficient with *Re* can be attributed to the increase of the heat transfer rate as a result of the increase of the air flow momentum. The decrease of the Colburn factor can be investigated based on the definition of the Colburn factor (Eqs. (12) and (13)). Increasing *Re* increases both of the heat transfer coefficient and the mass flux. The increase of the Colburn factor due to the increase of the heat transfer coefficient cannot overcome on the decrease of the Colburn factor due to the increase of the mass flux. This is supported

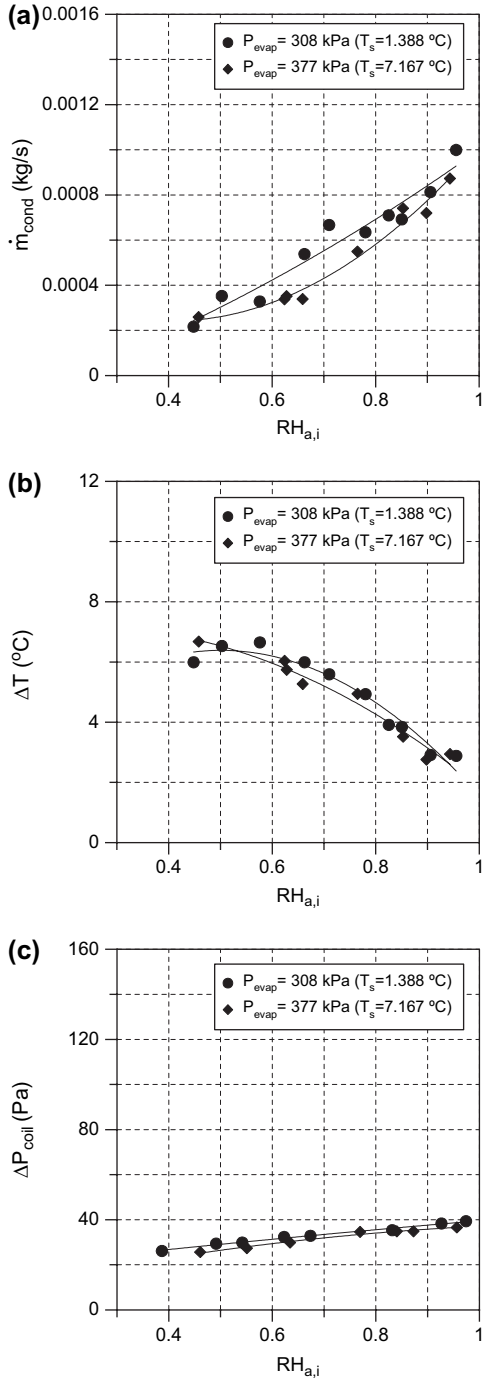

Fig. 6. Effect of evaporator pressure on (a) dehumidification capacity, (b) temperature drop across coil, and (c) air pressure drop across coil, at $V_{a,i} = 1$ m s^{-1} and $T_{a,i} = 20$ °C.

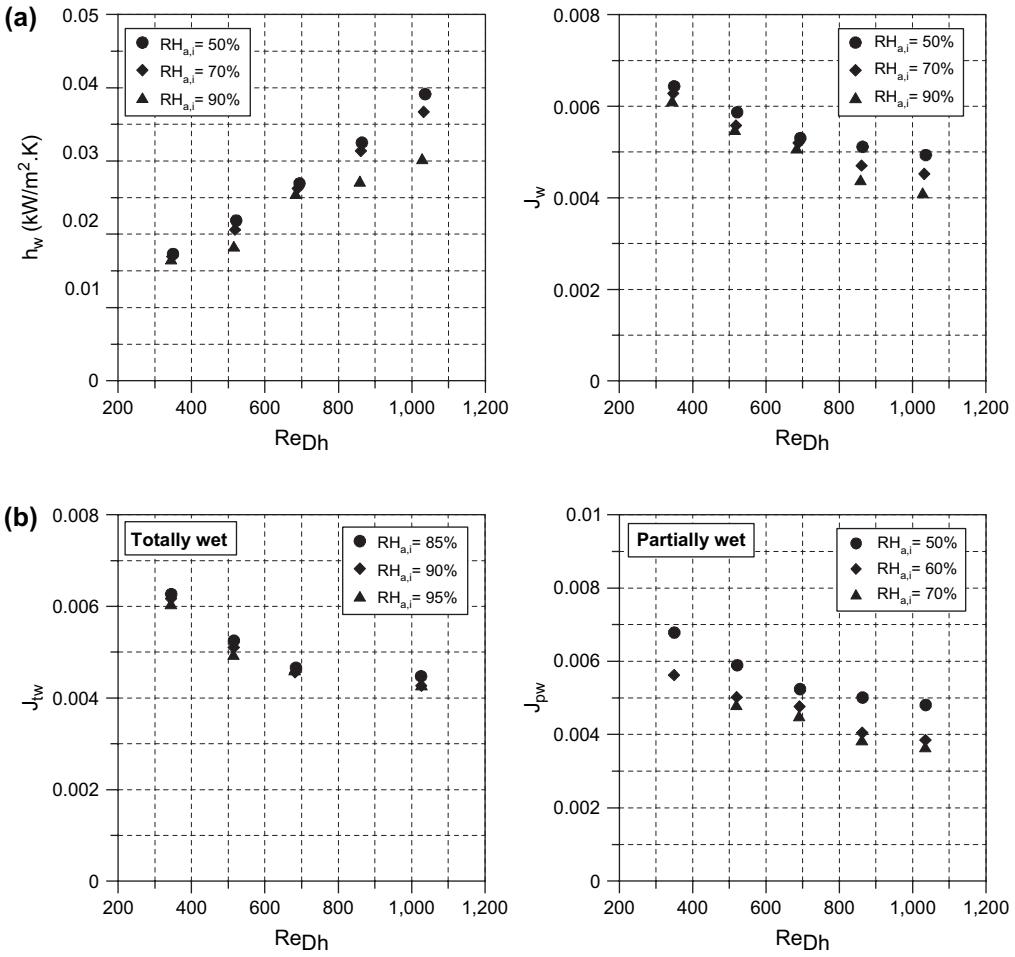

Fig. 7. Effect of $RH_{a,i}$ and Re on (a) h_w and J_w, and (b) J_{tw} and J_{pw} ($T_{a,i} = 20\,^{\circ}C$ at $P_{evap} = 308$ kPa).

by the results of Wang et al. [13] and Wang and Hihara [26] which showed the decrease of Colburn factor under dehumidification conditions with increasing Re.

The effects of the air inlet temperature on h_w, J_w, J_{tw} and J_{pw} are shown in Fig. 8 for specific values of $RH_{a,i}$ and P_{evap} (curves for other $RH_{a,i}$ and P_{evap} are given in Elattar [27]). As shown in Fig. 8, the Colburn factor slightly decreased as the air inlet temperature increased from 20 to 25 °C and it significantly decreased as the air inlet temperature increased from 25 to 30 °C. The trend was the same for all Reynolds numbers, air relative humidity and evaporator pressures. This trend can be attributed to the increase of the air inlet enthalpy with increasing the air inlet temperature for the same air inlet relative humidity. This causes an increase in $(i_{a,i} - i_s)$ and $(T_{a,ie} - T_s)$ which leads to a lower heat transfer coefficients and Colburn factors (see Eqs. (3), (9) and (10)).

Fig. 9 shows the effect of the evaporator pressure on h_w, J_w, J_{tw} and J_{pw} for different Reynolds numbers and at certain relative humidity and air temperature (curves for other $RH_{a,i}$ and $T_{a,i}$ are given in Elattar [27]). As shown in Fig. 9, the Colburn factor decreases with decreasing the evaporator pressure. The result is the same for all Reynolds numbers, relative humidity and air temperatures. This trend can be attributed to the decrease of the apparatus dew point with the decrease of the evaporator pressure. Decreasing the coil apparatus dew point causes an increase in $(i_{a,i} - i_s)$ and $(T_{a,ie} - T_s)$ and also an increase in the dehumidification capacity and these lead to a lower heat transfer coefficient and consequently lower Colburn factor.

The variation of the Colburn J factors, calculated from enthalpy potential method and EDT method, with Re, $RH_{a,i}$, $T_{a,i}$ and T_s are correlated as follows:

1. Enthalpy potential method

$$J = 0.029 Re^{-0.232} RH_{a,i}^{-0.35} \left(\frac{T_{a,i} - T_s}{T_s}\right)^{-0.18} \quad (15)$$

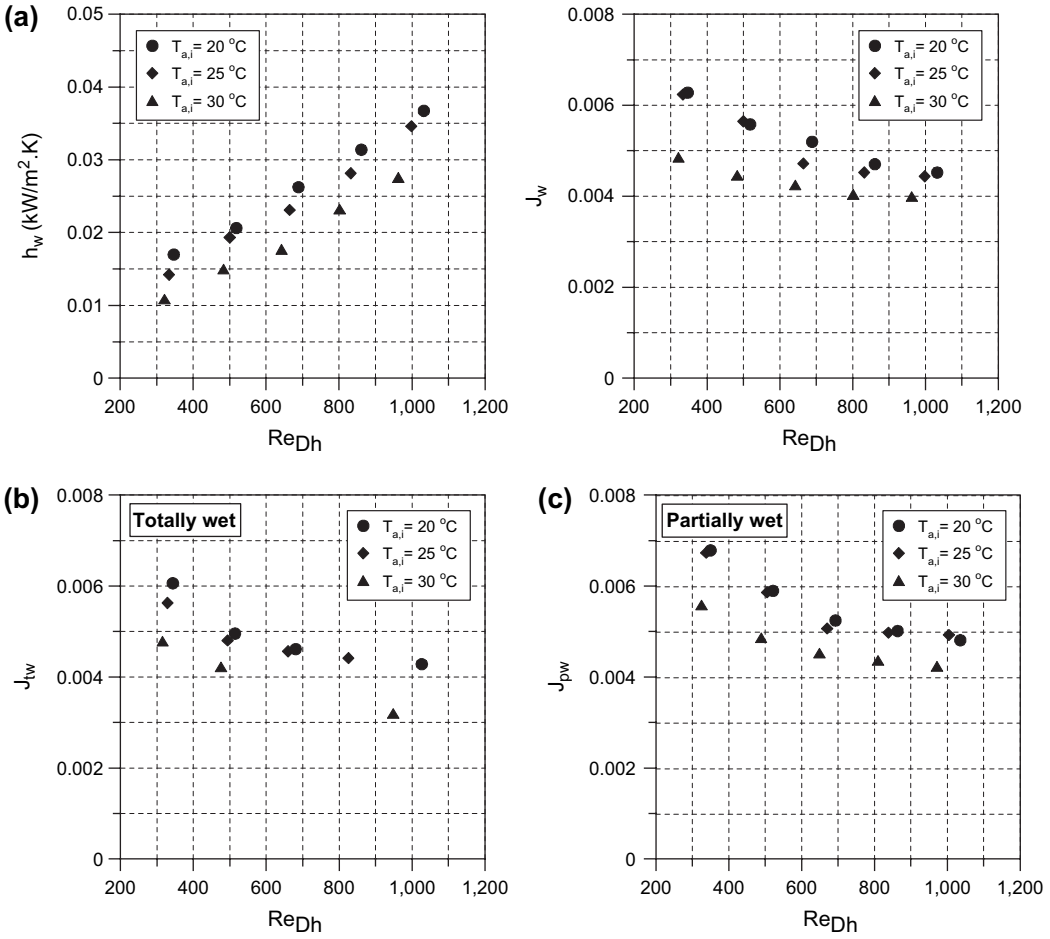

Fig. 8. Effect of air inlet temperature on h_w, J_{tw} and J_{pw} at $P_{evap} = 308$ kPa. (a) RH = 70%, (b) RH = 90%, and (c) RH = 50%.

Eq. (15) is correlated for data in the ranges: $300 \le Re \le 1050$, $50\% \le \mathrm{RH} \le 95\%$, $20\ ^\circ\mathrm{C} \le T_{a,i} \le 30\ ^\circ\mathrm{C}$ and $1.388\ ^\circ\mathrm{C} \le T_s \le 7.167\ ^\circ\mathrm{C}$.

2. EDT method; totally wet mode

$$J_{aw} = 0.044 Re^{-0.29} \mathrm{RH}_{a,i}^{-0.45} \left(\frac{T_{a,i} - T_s}{T_s}\right)^{-0.17} \quad (16)$$

3. EDT method; partially wet mode

$$J_{pw} = 0.029 Re^{-0.24} \mathrm{RH}_{a,i}^{-0.57} \left(\frac{T_{a,i} - T_s}{T_s}\right)^{-0.21} \quad (17)$$

Eqs. (16) and (17) are correlated for the data that lie in the totally wet and partly wet regions that were shown in Fig. 3, respectively. Comparison between the predictions of Eqs. (15), (16) and (17) and the present experimental data are shown in Fig. 10a–c, respectively. Regression analysis showed that Eqs. (15)–(17) predict all the experimental data within errors of ±21.6, ±17.48, and ±15.5% and predict 80% of the experimental data within ±14.23, ±10.37 and ±9.13%, respectively.

4.3. Evaluation and comparison of enthalpy potential and ETD method

From the discussion of Sections 4.1 and 4.2, we can conclude that: (1) in the enthalpy potential method, an unique correlation for the Colburn factor was proposed for all operating conditions, while for EDT method, two correlations are proposed, differentiated with respect to the wetting conditions; this gives an advantages of the enthalpy potential method over the EDT method, (2) it is obvious that the correlations predicted from the EDT method get closer to the experimental data; this gives an advantage of the EDT method over the enthalpy potential method, and (3) the EDT method requires the determination of the wetting conditions corresponding to the coil operating conditions from the cooling mode chart; this

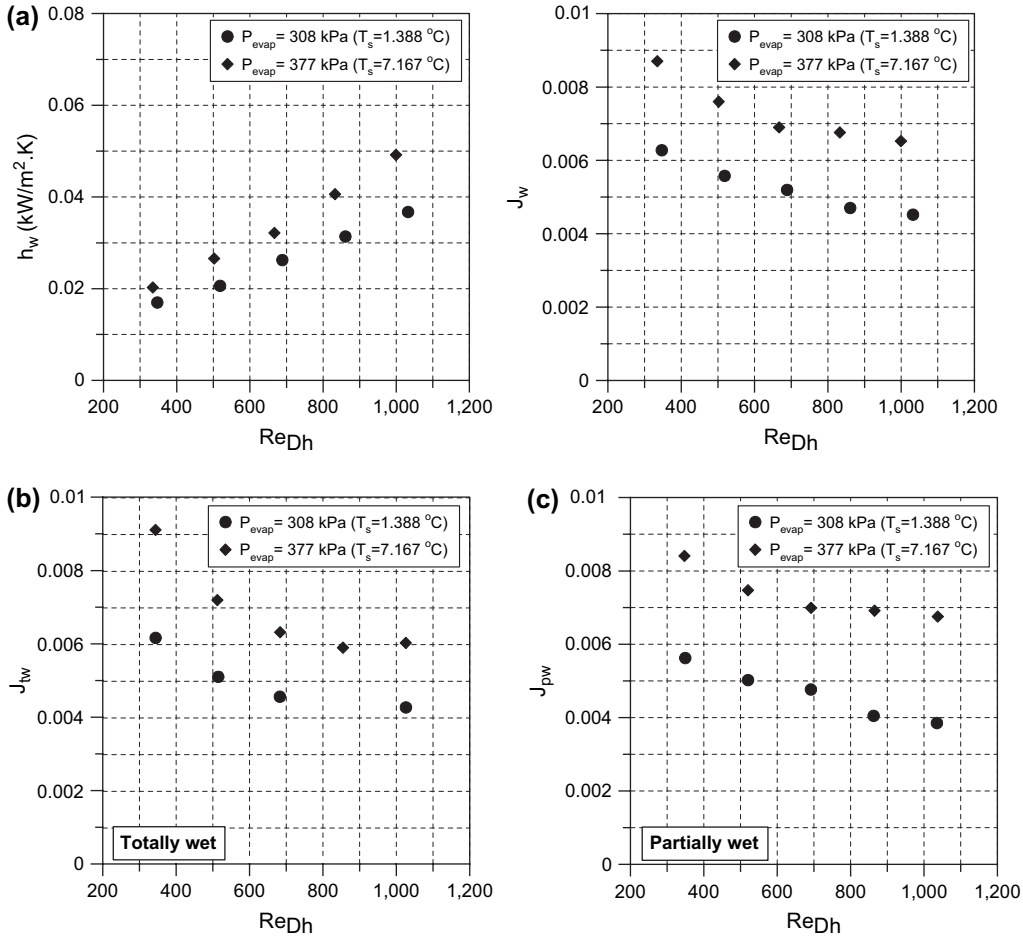

Fig. 9. Effect of evaporator pressure on h_w, J_{tw} and J_{pw} at $T_{a,i} = 20\,^{\circ}C$. (a) RH = 70%, (b) RH = 90%, and (c) RH = 60%.

gives disadvantages of the EDT method. Therefore, using the cooling modes chart (Fig. 3) to determine the cooling modes for a specified operating conditions and then using the correlation deduced from EDT method gives accurate value of J than using a correlation deduced from the enthalpy potential method. On the other hand if the cooling mode chart is not available, a correlation deduced from the enthalpy potential method can be used to predict the heat transfer coefficient with larger but acceptable error.

5. Comparison with previous work

As shown in Section 4.2, the Colburn J factor depends on the operating conditions. Also it is known from the literature review that the Colburn J factor depends on the coil geometrical parameters. To the author's knowledge no experimental works about the performance of wavy-finned-tube D-X cooling and dehumidifying coil under the geometric and operating conditions of the present study are available on the open literature. Moreover, using the EDT method to measure the performance of the cooling coils under different coil wetting conditions have not been used until now. Therefore, quantitative comparison of the present work with previous works is difficult. However, the trend of J_w of the present data can be compared in Fig. 11 with the trends of the data of Halici et al. [15], Wang et al. [13] and Wang et al. [29]. In these studies chilled water cooling and dehumidifying coils were used. As shown in the figure, all trends show the decrease of J_w with increasing Reynolds number. Also the figure shows that the data of Halici et al. [15] and Wang et al. [13] are significantly higher than the present data while the data of Wang et al. [29] is closer to the present data. This may be attributed to that the work of Halici et al. [15] and Wang et al. [13] were carried out on a flat-plate-finned tube coil, while the work of Wang et al. [29] was carried out on a wavy-finned tube air coil, as the present study but for different coil geometrical parameters.

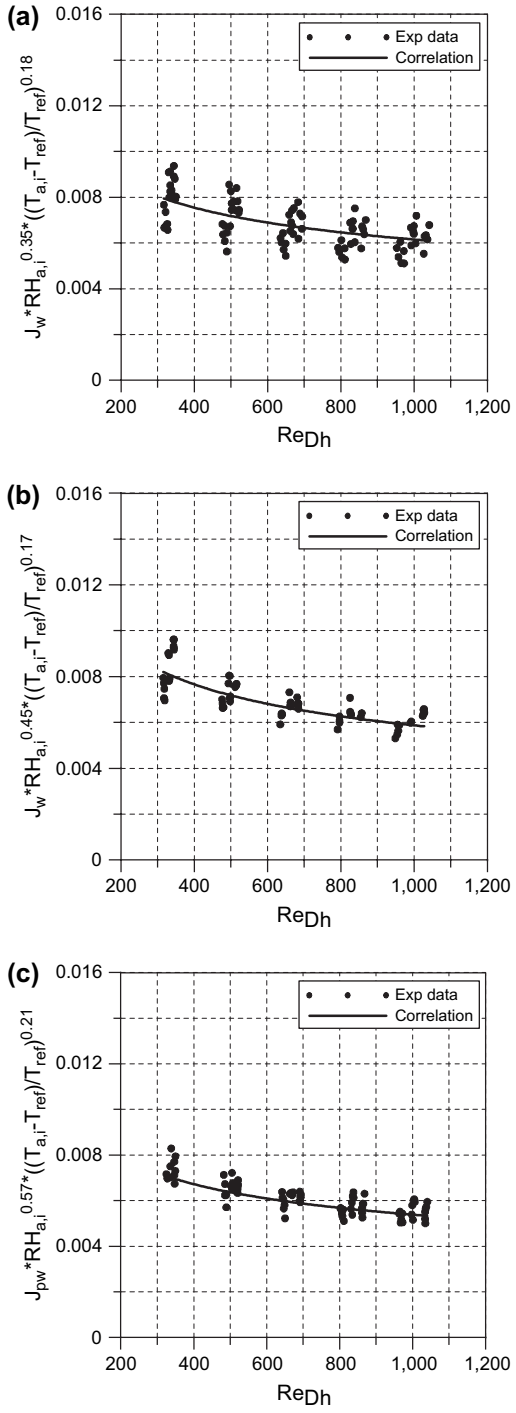

Fig. 10. Predictions of Eqs. (15)–(17). (a) Eq. (15), (b) Eq. (16), and (c) Eq. (17).

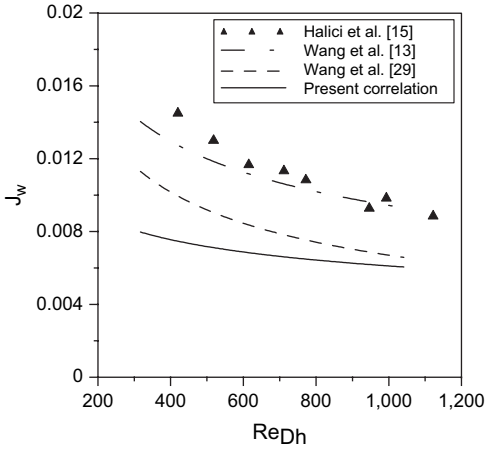

Fig. 11. Comparison of present results with previous works.

6. Summary and conclusions

An experimental investigation of the airside performance of a wavy-finned-tube direct expansion air coil under dehumidification condition using R134a as a refrigerant was presented. The effects of the air inlet Psychrometric properties (air inlet temperature and air inlet relative humidity), Reynolds number and the coil pressure on the heat/mass transfer and the pressure drop characteristics were investigated. The results showed that: (1) the air temperature drop across the coil decreases with increasing the air inlet relative humidity, the air coil face velocity, and the air inlet temperature, (2) the dehumidification capacity increases with increasing the air inlet relative humidity, the coil face velocity, and the air inlet temperature and decreases with increasing the evaporator pressure, and (3) the pressure drop across the coil increases with increasing both of the air inlet relative humidity and the coil face velocity and was insensitive to the air inlet temperature and the coil pressure. The airside thermal performance of the coil was analyzed using two different techniques; the enthalpy potential method and the equivalent dry-bulb temperature (EDT) method. In the first technique, the Colburn J factor under wet condition was calculated regardless the coil wet conditions (partially wet or totally wet), while in the second technique, cooling and dehumidification modes charts were firstly proposed to classify the data to two groups; group for totally wet coil condition data and group for partially wet coil condition data. The Colburn J factor for each group was calculated using different method of analysis. The two techniques showed that the Colburn J factor decreases with increasing Re, relative humidity and air inlet temperature. Correlations for the Colburn J factor using enthalpy potential and EDT analysis methods were developed in terms of Reynolds number, air inlet relative humidity, air inlet temperature

and refrigerant saturation temperature. The analysis showed that the prediction of the EDT method is closer to the experimental data than the prediction of the enthalpy potential method.

References

[1] Q. Xiao, W.Q. Tao, Effect of fin spacing on heat transfer and pressure drop of two-row corrugated-fin and tube heat exchangers, Int. Commun. Heat Mass Transf. 17 (1990) 577–586.

[2] J.Y. Jang, L.K. Chen, Numerical analysis of heat transfer and fluid flow in a three-dimensional wavy-fin and tube heat exchanger, Int. J. Heat Mass Transf. 40 (1997) 3981–3990.

[3] C.C. Wang, W.L. Fu, C.T. Chang, Heat transfer and friction characteristics of typical wavy fin-and-tube heat exchangers, Exp. Therm. Fluid Sci. 14 (1997) 174–186.

[4] C.C. Wang, Y.M. Tsai, D.C. Lu, Comprehensive study of convex-louver and wavy fin-and-tube heat exchangers, J. Thermophys. Heat Transf. 12 (1998) 423–430.

[5] M.A. Madi, R.A. Johns, M.R. Heikal, Performance characteristics correlation for round tube and plate finned heat exchangers, Int. J. Refrigeration 21 (1998) 507–517.

[6] C.C. Wang, J.W. Jang, N.F. Chiou, A heat transfer and friction correlation for wavy fin-and-tube heat exchangers, Int. J. Heat Mass Transf. 42 (1999) 1919–1924.

[7] C.C. Wang, Y.M. Hwang, Y.T. Lin, Empirical correlations for heat transfer and flow friction characteristics of herringbone wavy fin-and-tube heat exchangers, Int. J. Refrigeration 25 (2002) 673–680.

[8] S. Wongwises, Y. Chokeman, Effect of fin pitch and number of tube rows on the air side performance of herringbone wavy fin and tube heat exchangers, Energy Convers. Manag. 46 (2005) 2216–2231.

[9] Y. Seshimo, K. Ogawa, K. Marumoto, M. Fujii, Heat and Mass Transfer Performances on Plate Fin and Tube Heat Exchangers with Dehumidification, Mitsubishi Electric Corp., Scriptaa Technica, Inc., 1989, pp. 79–94.

[10] H. Kazeminejad, Analysis of one-dimensional fin assembly heat transfer with dehumidification, Int. J. Heat Mass Transf. 39 (1995) 455–462.

[11] S.A. Idem, A.M. Jacobi, V.W. Goldschmidt, Heat transfer characterization of a finned-tube heat exchanger (with and without condensation), ASME J. Heat Transf. 112 (1990) 64–70.

[12] C.C. Wang, Y.C. Hsieh, Y.T. Lin, Performance of plate finned tube heat exchangers under dehumidifying conditions, ASME J Heat Transf. 119 (1997) 109–117.

[13] C.C. Wang, Y.T. Lin, C.J. Lee, An airside correlation for plain fin-and-tube heat exchangers in wet conditions, Int. J. Heat Mass Transf. 43 (2000) 1869–1872.

[14] Y. Yao, Z. Lian, Z. Hou, Thermal analysis of cooling coils based on a dynamic model, Appl. Therm. Eng. 24 (2004) 1037–1050.

[15] F. Halici, I. Taymaz, M. Gunduz, The effect of the number of tube rows on heat, mass and momentum transfer in flat-plate finned tube heat exchangers, Energy 26 (2001) 963–972.

[16] M.H. Kim, C.W. Bullard, Air-side performance of brazed aluminum heat exchangers under dehumidifying conditions, Int. J. Refrigeration 25 (2002) 924–934.

[17] S. Theerakulpisut, S. Priperm, Modeling cooling coils, Int. Commun. Heat Mass Transf. 25 (1998) 127–137.

[18] D.R. Mirth, S. Ramadhyani, Prediction of cooling-coil performance under condensing conditions, Int. J. Heat Fluid Flow 14 (4) (1993) 391–400.

[19] D.R. Mirth, S. Ramadhyani, Performance of chilled-water cooling coils, HVAC&R Res 1 (1995) 160–171.

[20] Y.T. Lin, Y.M. Hwang, C.C. Wang, Performance of the herringbone wavy fin under dehumidifying conditions, Int. J. Heat Mass Transf. 45 (2002) 5035–5044.

[21] J. Threlkeld, Thermal Environmental Engineering, Prentice-Hall, Englewood Cliffs, New Jersey, 1970.

[22] H. Kazeminejad, M.A. Yaghoubi, F. Bahri, Conjugate forced convection–conduction analysis of the performance of a cooling and dehumidifying vertical rectangular fin, Int. J. Heat Mass Transf. 36 (1993) 3625–3631.

[23] K.T. Hong, R.L. Webb, Calculation of fin efficiency for wet and dry fins, HVAC&R Res 2 (1) (1996) 27–41.

[24] B. Kundu, An analytical study of the effect of dehumidification of air on the performance and optimization of straight tapered fins, Int. Commun. Heat Mass Transf. 29 (2) (2002) 269–278.

[25] S.Y. Liang, M. Liu, T.N. Wong, G.K. Nathan, Analytical study of evaporator coil in humid environment, Appl. Therm. Eng. 19 (1999) 1129–1145.

[26] J. Wang, E. Hihara, Prediction of air coil performance under partially wet and totally wet cooling conditions using equivalent dry-bulb-temperature method, Int. J. Refrigeration 26 (2003) 293–301.

[27] H.F. Elattar, Performance of a Wavy-Finned-Tube Direct Expansion Cooling and Dehumidifying Coil, M.Sc. thesis, Benha High Institute of Technology, Benha, Egypt, 2006.

[28] J.P. Holman, W.J. Gajda, Experimental Method for Engineers, McGraw Hill, New York, 1994.

[29] C.C. Wang, Y.J. Du, Y.J. Chang, W.H. Tao, Airside performance of herringbone fin-and-tube heat exchangers in wet conditions, Can. J. Chem. Eng. 77 (6) (1999) 1225–1230.